Journal of Pharmaceutical and Biomedical Analysis 102 (2015) 129–136

Contents lists available at ScienceDirect

Journal of Pharmaceutical and Biomedical Analysis

journal homepage: www.elsevier.com/locate/jpba

Quantitative detection of drug dose and spatial distribution in the lung revealed by Cryoslicing Imaging

Nirav Barapatre[a,b], Panagiotis Symvoulidis[d], Winfried Möller[a,b], Friedrich Prade[a,b], Nikolaos C. Deliolanis[d,e], Sebastian Hertel[f,a,b], Gerhard Winter[f], Ali Ö. Yildirim[a,b], Tobias Stoeger[a,b], Oliver Eickelberg[a,b,c], Vasilis Ntziachristos[d], Otmar Schmid[a,b,*]

[a] Comprehensive Pneumology Center, Member of the German Center for Lung Research, Max-Lebsche-Platz 31, 81377 Munich, Germany
[b] Institute of Lung Biology and Disease, Helmholtz Zentrum München, 85764 Neuherberg, Germany
[c] University Hospital, Ludwig-Maximilians-University, Marchioninistraße 15, 81377 Munich, Germany
[d] Institute of Biological and Medical Imaging, Helmholtz Zentrum München and Technische Universität München, 85764 Neuherberg, Germany
[e] Fraunhofer Project Group for Automation in Medicine and Biotechnology, 68167 Mannheim, Germany
[f] Department of Pharmacy, Pharmaceutical Technology and Biopharmacy, Ludwig-Maximilians-University, 81377 Munich, Germany

ARTICLE INFO

Article history:
Received 25 April 2014
Received in revised form 6 August 2014
Accepted 1 September 2014
Available online 8 September 2014

Keywords:
Cryoslicing Imaging
Drug delivery
Fluorescence
Mouse model
Tissue attenuation coefficient

ABSTRACT

Administration of drugs *via* inhalation is an attractive route for pulmonary and systemic drug delivery. The therapeutic outcome of inhalation therapy depends not only on the dose of the lung-delivered drug, but also on its bioactivity and regional distribution. Fluorescence imaging has the potential to monitor these aspects already during preclinical development of inhaled drugs, but quantitative methods of analysis are lacking. In this proof-of-concept study, we demonstrate that Cryoslicing Imaging allows for 3D quantitative fluorescence imaging on *ex vivo* murine lungs. Known amounts of fluorescent substance (nanoparticles or fluorophore–drug conjugate) were instilled in the lungs of mice. The excised lungs were measured by Cryoslicing Imaging. Herein, white light and fluorescence images are obtained from the face of a gradually sliced frozen organ block. A quantitative representation of the fluorescence intensity throughout the lung was inferred from the images by accounting for instrument noise, tissue autofluorescence and out-of-plane fluorescence. Importantly, the out-of-plane fluorescence correction is based on the experimentally determined effective light attenuation coefficient of frozen murine lung tissue ($10.0 \pm 0.6\,cm^{-1}$ at 716 nm). The linear correlation between pulmonary total fluorescence intensity and pulmonary fluorophore dose indicates the validity of this method and allows direct fluorophore dose assessment. The pulmonary dose of a fluorescence-labeled drug (FcγR-Alexa750) could be assessed with an estimated accuracy of 9% and the limit of detection in ng regime. Hence, Cryoslicing Imaging can be used for quantitative assessment of dose and 3D distribution of fluorescence-labeled drugs or drug carriers in the lungs of mice.

1. Introduction

Inhalation is a promising route for rapid and non-invasive delivery of aerosolized therapeutics to the lungs and other target organs. Inhalation therapy is ideally suited for treating lung diseases as it allows for delivery of drugs directly to the site of action. This minimizes side effects and enables immediate drug action at the diseased tissue. In addition, the large surface area of the lung (*ca.* 70 m^2), the highly dispersed nature of an inhaled aerosol and the good permeability of the alveolar air–blood barrier allow for rapid transport of small molecules from the lung to other organs *via* systemic circulation [1]. Particularly for drugs with poor oral bioavailability, such as peptides and proteins, the pulmonary route offers a promising alternative way of systemic drug delivery [2]. The avoidance of hepatic and intestinal first-pass metabolism is an added benefit of pulmonary drug delivery compared to oral application.

Depending on the type of disease, the drug should be targeted to specific regions of the lung. For instance, asthma attacks are mainly

* Corresponding author at: Helmholtz Zentrum München, German Research Center for Environmental Health, Institute of Lung Biology and Disease, Ingolstädter Landstr. 1, 85764 Neuherberg, Germany. Tel.: +49 8931872557; fax: +49 8931872400.
E-mail address: otmar.schmid@helmholtz-muenchen.de (O. Schmid).

http://dx.doi.org/10.1016/j.jpba.2014.09.001

due to severe bronchial constriction, while lung emphysema is characterized by a loss of alveolar septa. Hence, the therapeutic outcome of inhalation therapy depends not only on lung-delivered drug dose, but also on the regional distribution (*e.g.* airways *versus* alveoli) and bioactivity of the delivered drug [3,4]. These aspects should already be considered during the preclinical development of inhaled drugs [5,6]. Hence, preclinical methods for detection of pulmonary dose, spatial distribution and bioactivity of the drug are required. Radioactive labeling allows for regional dosimetry *via* X-ray tomography (CT), PET and SPECT, but not for determination of the bioactivity of the substances. On the other hand, fluorescent substances including nanoparticles have been widely used for preclinical dosimetry studies both *in vitro* and *in vivo* [7,8] and numerous fluorescent probes are available for studying the bioactivity of drugs in terms of activation/deactivation of complex biological processes in living animals. Consequently, using innovative preclinical strategies of optical imaging has allowed *in vivo* real-time insight not only in genomics and proteomics ([9] and references 1–6 herein), but also in disease state of animal models such as the size of cancer lesions or of a remodeled bone [10].

However, one of the main drawbacks of *in vivo* optical imaging is the significant interaction of light with biological tissue due to scattering and absorption resulting in significant light attenuation, blurring and halo effects. This limits the applicability of optical imaging to a depth of a few millimeters or less, especially outside the so-called *optical window* in the near infrared (NIR) wavelength regime (≈600–1000 nm), where light–tissue interaction is minimal [11]. This significantly hampers the possibility of deriving quantitative information on dose and/or biological response from optical imaging methods [12,13]. Consequently, only a few attempts have been published, where quantitative information on biological processes or disease state has been obtained from inner organs of small animals [10]. Compared to all other internal organs, light propagation through the lung is further complicated by the interaction of light with the numerous air–tissue interfaces due to millions of alveolar sacks comprising about 90% of the lung volume. This makes quantitative *in vivo* fluorescence imaging in the lungs even more elusive.

Cryoslicing Imaging has been used as an alternative to *in vivo* imaging. Herein, a frozen specimen block is imaged and sliced in an alternate manner as depicted in Fig. A.1 (online supplement). As the lung has to be excised Cryoslicing Imaging is a time-consuming, terminal procedure, but it provides much better spatial resolution and can serve as a quantitative verification of the *in vivo* imaging results [14]. Similar systems of varying measurement capabilities, spatial resolution and sensitivity have been used in the past for validation of novel imaging modalities like near-field thermo-acoustic imaging [15] and fluorescence molecular tomography [10], for anatomical visualization of intramural coronary vasculature [16], to study bio-distribution of molecular probes [17] or GFP-labeled cancer cells [14], and for single cell visualization and quantification [18].

In this study we describe and validate a Cryoslicing Imaging method for quantitative assessment of 3D dose distribution of fluorescent substances in the lungs of mice. The main components of the method are dose-controlled *in vivo* administration of a fluorescent substance into the lungs, sample (lung) preparation as well as acquisition and processing of the images. For conversion of block face images into single-slice fluorescence images, the effective attenuation coefficient of frozen (murine) lung tissue was experimentally determined and used to account for out-of-plane fluorescence in the block face images. The Cryoslicing Imaging method is validated by linear dose–response curves from lungs of mice with known amounts of fluorescent nanoparticles and a fluorescence-labeled, molecular drug currently undergoing preclinical testing.

2. Material and methods

2.1. Fluorescent substances

For validation of the Cryoslicing Imaging method presented here known amounts of fluorophore were delivered directly to the lungs of mice by intratracheal instillation as described below. Two types of fluorescent substances were used for the experiments, namely polystyrene nanoparticles (diameter 450 nm) with the embedded fluorescent dye Sky Blue (excitation/emission = 670 nm/710 nm; Kisker Biotech GmbH, Steinfurt, Germany) and a molecular drug (soluble human Fcγ receptor IIB) covalently bound to the fluorophore Alexa750 (Ex/Em = 749 nm/775 nm), henceforth referred to as FcγR-Alexa750. Four different concentrations (1:20, 1:60, 1:200 and 1:600 dilutions) of a 1 mg/ml Sky Blue stock solution were prepared in pyrogene-free distilled water for intratracheal instillation in mice. Similarly, two different dilutions (1:20 and 1:40) of a 1 mg/ml stock solution of FcγR-Alexa750 were prepared in phosphate buffered saline.

2.2. Animal handling and preparation of the lung

Mice were kept in isolated ventilated cages (IVC-Racks; BioZone, Margate, UK) supplied with filtered air in a 12-h light/12-h dark cycle (lights on from 06:00–18:00). Food (standard chow) and water were available *ad libitum*. All procedures for animal handling and experiments were performed in accordance with protocols approved by the Regierung von Oberbayern (District Government of Upper Bavaria).

Six FVB-GT mice (13–19 weeks, 2 male, 4 female, 25–35 g) and seven C57BL/6 mice (age 8–14 weeks, all female, weight 18–27 g) were used for experiments with Sky Blue and FcγR-Alexa750, respectively. For each mouse strain two animals were selected as control mice (without fluorophore). One FVB-GT mouse was not successfully instilled and hence discarded. Prior to instillation, mice were anesthetized by intraperitoneal injection of a mixture of medetomidine (0.5 mg/kg body mass), midazolam (5.0 mg/kg body mass) and fentanyl (0.05 mg/kg body mass). Animals were then intubated by a non-surgical technique [19]. A 20G cannula (Cat. No. 4254112B, B. Braun, Melsungen, Germany) was inserted 10 mm into the trachea and correct placement of the cannula in the trachea instead of the esophagus was verified with a pneumotachograph. Subsequently, a 1 ml syringe containing 50 μl of fluorophore solution/suspension and 200 μl of air was connected to the cannula and squirted directly into the lungs by intratracheal instillation as the animal inhaled [20]. The 200 μl of air facilitates transport of the 50 μl of liquid into the lung. The actually delivered pulmonary fluorophore dose of 38.6 ± 5.5 μl (mean ± standard deviation; or ±14.2% relative standard deviation) was measured by weighing the cannula and the syringe before and after the delivery. Thus, on average only 76% of the invested dose reached the lung, while the rest remained in the instillation wear and the uncertainty in pulmonary substance dose would be 14.2%, if the gravimetric analysis of the instillation wear would not have been performed. Here, the accuracy of the delivered dose is estimated to be 5% mainly due to inadvertent loss of small amounts of liquid during handling of the instillation wear. The maximum instilled mass of dye instilled into the lungs was 1.9 μg (=38.6 μl out of a 1:20 diluted 1 mg/ml stock solution).

The anesthetized mice were sacrificed immediately after the application procedure by exsanguination. Subsequently, a 21G cannula was inserted into the trachea by tracheotomy, the lung was removed from the animal chest, and the lung was partially inflated by connecting an OCT-filled syringe (Tissue Tek Optimal Cutting Temperature compound, VWR International GmbH, Darmstadt, Germany) to the cannula and gently infusing 0.5 ml of clear OCT.

Apart from preventing the lung from collapsing, the OCT infusion also provides a stable substrate for cryoslicing. The lung was then embedded into a 30 mm diameter cylindrical block using black pigmented OCT and placed into a –20 °C freezer. The black pigmented OCT reduced scattering of light from the surrounding OCT into the lung tissue and simplified automated selection of lung area during quantitative region-of-interest (ROI) analysis. The lung blocks were measured in the frozen state by Cryoslicing Imaging. The block face was imaged at every 100 μm step. The slicing thickness was chosen at 25 μm to maintain the sample integrity. Hence, four slicing steps were performed between two consecutive images.

2.3. Image processing

Quantitative analysis of the fluorescence images requires careful consideration of measurement biases, out-of-plane fluorescence and optical properties of the lung tissue.

2.3.1. Background noise subtraction

As with any fluorescence imaging system, multiple types of scene-, pixel-, and exposure-time-dependent noise and parasitic signals contributed to the actual image, including noise from the CCD sensor, ambient light at the emission wavelength, cross-talk of the filters, lens imperfections, and tissue auto-fluorescence. Four lungs with no application of fluorophores (untreated lungs) were measured with the same setup to account for these biases (systematic biases) and to determine the lower limit of detection (statistical noise). The exposure time of the camera was kept variable to provide optimum signal-to-noise ratio for images with low and high signal intensity. The contribution of background signal was determined by taking a mean photon count from the corners of the fluorescence images devoid of any specimen structures. The mean background counts were found to be linearly dependent on the exposure time of each image. The offset of the linear fit was assumed to be the additive noise (electronic read-out bias and dark current). In order to achieve quantitative fluorophore assessment, bias corrections and block face to slice intensity inversion were done with an image processing routine written in MATLAB.

As seen in Eq. (1) the exposure-time-dependent background signal and the electronic noise ($F_{noise}(t_{exp})$) were subtracted from each fluorescence block face image (F_{meas}) and then normalized to the exposure time (t_{exp})

$$F_{cor} = \frac{F_{meas} - F_{noise}(t_{\exp})}{t_{\exp}} \quad (1)$$

yielding fluorescence photon counts per second as new intensity signal.

2.3.2. Out-of-plane fluorescence subtraction

The sequence of corrected block face images was inverted into single slice images by subtracting out-of-plane fluorescence from the block face images according to an empirical algorithm described by [18]. Briefly, if F_n and F_{n-1} represent consecutive corrected block face images (Eq. (1)), the fluorescence image attributed to fluorophore located in the nth lung slice (S_n) can be calculated according to

$$S_n = F_n - F_{n-1} \exp(-\mu_{\text{eff}} d), \quad (2)$$

where d and μ_{eff} are the layer thickness (here: 100 μm) and the effective attenuation coefficient of frozen lung tissue, respectively. The exponential factor in Eq. (2) accounts for light attenuation of out-of-plane fluorescence within the nth layer according to Lambert–Beer's law. The stack of single slice images S_n represents the fluorophore-induced fluorescence intensities throughout the entire lung. The dose of the fluorescent marker in the whole lung should be proportional to the sum of the fluorescence intensities from all 100 μm slices $\left(\sum_n S_n\right)$. The conversion factor relating measured fluorescence intensity to fluorophore mass can be determined experimentally as described below. For reconstruction and visualization of 3D distributions of the fluorophore in the lungs ImageJ and Amira software products were used. The μ_{eff} of the frozen lung tissue was obtained experimentally by implanting a fluorescent point source in an excised murine lung as described in the online supplement.

2.4. Determination of the intensity–dose conversion factor

As mentioned above, conversion of the measured total fluorophore intensity from all tissue slices into pulmonary fluorophore mass requires experimental determination of an intensity–mass conversion factor. This can be accomplished by preparing multiple lungs containing known but different amount of fluorophore doses. After processing the lungs as described above the measured total fluorophore intensity can be related to known fluorophore doses yielding the desired intensity–mass conversion factor for quantitative Cryoslicing Imaging. If the relationship is linear then the intensity–mass conversion factor can be obtained by using just two "reference" lungs, one containing a realistically distributed and known amount of fluorophore and one without any fluorophore (autofluorescence of tissue). Of course, using a larger number of reference lungs will improve the dosimetric accuracy of the method. Finally, the measured 3D intensity map is converted into a 3D fluorophore dose distribution by pixel-wise multiplication of the intensity map with the intensity–mass conversion factor.

3. Results

3.1. Lung Cryoslicing Imaging

The apparatus used for Cryoslicing Imaging of the lung is described in the online supplement and illustrated in Fig. A.1. In Cryoslicing Imaging the visualization of the fluorophore distribution in 3D is achieved by stacking the serial fluorescence block face images of the specimen. Fig. 1a shows a reconstructed frontal lung slice along the trachea, *i.e.* in a direction perpendicular to

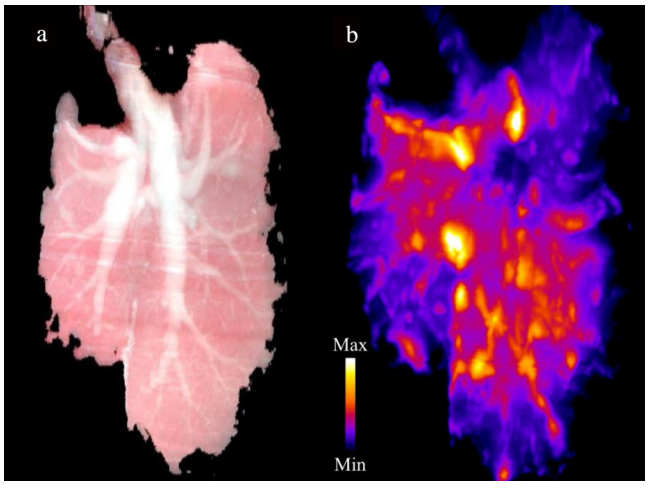

Fig. 1. 2D projection of 3D distribution of the fluorophore. (a) Frontal slice of the lung along the trachea obtained from 3D reconstruction using the axial white light reflection slices. The white region shows OCT injected into the airways of the excised lung (the outside-lung background was removed using an automated mask). (b) Reconstructed distribution of FcγR-Alexa750 as a 3D maximum intensity projection of the fluorescence channels corresponding to the view presented in panel (a). This indicates the pulmonary distribution of the fluorescence-labeled dye after intratracheal instillation into the lung.

the cutting and imaging during block face imaging. This image is obtained from frontal re-construction of the measured axial RGB (red–green–blue, *i.e.* white light) reflection images. White color in the airways is due to unpigmented OCT instilled in the lungs during cryofixation. The image clearly illustrates the left and the right half of the lung and their typical monopodal airway structure (small airways branching-off one main airway). Fig. 1b shows the associated frontal re-construction of the 3D fluorescence marker distribution for the lung. It depicts a maximum intensity projection of the fluorescence channel, where increasing brightness correlates with enhanced fluorescence-labeled drug dose. As seen from Fig. 1b application of fluorophore by intratracheal instillation preferentially targets the central airways of the lung.

3.2. Experimental determination of the effective attenuation coefficient of lung tissue

As mentioned above for quantitative fluorescence analysis the block face images have to be inverted into single slice images taking into account out-of-plane fluorescence, which requires knowledge of the effective attenuation coefficient (μ_{eff}) of the sample tissue (Eq. (2)). Fig. A.2 (online supplement) shows the decreasing block face intensity with increasing distance (100 μm increments) from a fluorescent point source due to tissue attenuation. Modeling light attenuation in frozen lung tissue according to Beer's law (exponential decay of intensity with increasing distance), μ_{eff} was derived from an exponential fit of the data. The resulting μ_{eff} value of $10.0 \pm 0.6\,cm^{-1}$ (at 716 nm) represents the sum of the excitation and the emission attenuation. It also implies that 90.5% (=exp($-10.0\,cm^{-1} \cdot 0.01$ cm)) of the fluorescence intensity emitted from the sub-surface layer (F_{n-1}) is reaching the surface of the organ block (Eq. (2)). Consequently, provided the fluorophore is uniformly distributed, about 90% of the measured block face fluorescence intensity (F_n) is due to sub-surface fluorescence and only 10% is emitted from the 100 μm thick surface layer.

3.3. Out-of-plane fluorescence correction of block face images

The sequence of block face images was inverted into single slice images by subtracting out-of-plane fluorescence from the block face images as described in Section 2. The tissue attenuation was taken into account with $\mu_{eff} = 10.0 \pm 0.6\,cm^{-1}$ (at 716 nm). The axial distribution of the fluorophore throughout the lung is illustrated in Fig. 2. The solid line depicts the measured total (sum over all pixels) block face intensity as the lung is sliced axially. The dotted line represents the net fluorescence from each 100 μm thick slice calculated from the block face images using Eq. (2) with $\mu_{eff} = 10.0 \pm 0.6\,cm^{-1}$. Evidently, both curves show a pronounced, broad peak in the central part of the lung, which is largely due to the increased cross-sectional area about half way between trachea and tip of the lung. Furthermore, Fig. 2 shows that about 90% of the measured block face light intensity is due to sub-surface light emission.

Fig. 3 compares the spatial distribution of the sub-surface corrected fluorescence intensity in a 100 μm slice (Fig. 3c) with the measured fluorescence intensity distribution in a single 25 μm slice (Fig. 3d) of the same block position. Fig. 3d was obtained with a different epi-fluorescence imaging system. During the slicing step a 25 μm slice was taken on a glass slide and imaged at room temperature. Fig. 3c was obtained by attenuating the F_{n-1} block face image ($\mu_{eff} = 10.0\,cm^{-1}$) and blurring it by a 10 pixel (360 μm) wide Gaussian kernel prior to subtracting it from the F_n block face image (Fig. 3b). The degree of blurring was experimentally determined by adjusting the Gaussian kernel such that any fluorescence signal from the OCT covered (normally air-filled) regions of the airways (identified from Fig. 3a) is eliminated. This approach utilizes

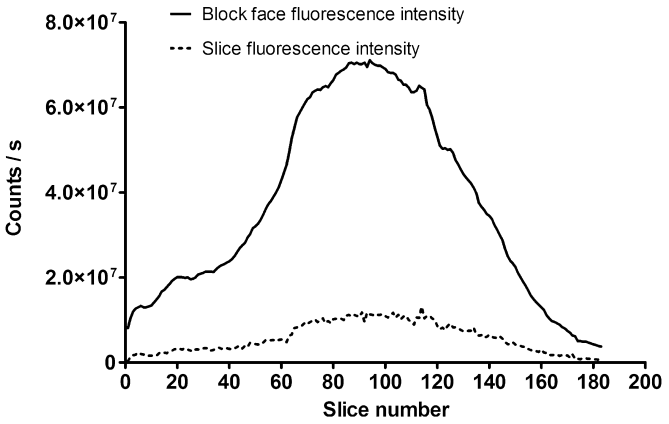

Fig. 2. Comparison of the measured fluorescence intensity in the block face to the calculated fluorescence intensity per slice. The solid line depicts the measured total (sum over all pixels) block face intensity as the lung is sliced axially. The dotted line represents the net fluorescence from each 100 μm thick slice calculated from the block face images using sub-surface correction according to Eq. (2) with $\mu_{eff} = 10.0 \pm 0.6\,cm^{-1}$. The lung was sliced axially along the orientation of the trachea starting from the trachea. Clearly, about 90% of the block face fluorescence intensity of FcγR-Alexa750 is due to sub-surface fluorescence and only about 10% of the measured light emanates from the top 100 μm thick slice. The elevated fluorescence levels between 65 and 120 are largely explained by the larger cross-sectional area of the lung in this region.

the fact that after subtraction of sub-surface fluorescence the airways should not show any fluorescence signal, as the fluorophore is deposited on the airway walls and/or is transported deeper into the tissue, but is not present in the airspace itself. Both the calculated 100 μm (Fig. 3c) and the directly measured 25 μm slice image (Fig. 3d) show a similar fluorophore intensity distribution with more pronounced fluorescence in the left half of the lung and a similar "hot spot" pattern. However, not all of the hot spots are matching up and most of the elevated fluorescence traces along some of the airway channels in Fig. 3c are not seen in Fig. 3d. This may be a result of the difference in layer thickness. If airways are 25–100 μm large, slicing off a 100 μm layer may completely eliminate the airway fluorescence in the F_{n-1} image. Conversely, the direct image from a 25 μm slice may not capture any of the fluorophore covering the airway walls. Interestingly, there are also some cases where fluorescent airway traces can be seen in both Fig. 3c and d suggesting that in this case the remainder of the airway was less than 25 μm deep.

3.4. Dose–response assessment

Fig. 4a shows the total pulmonary fluorescence intensity as a function of the intratracheally instilled mass of the fluorescent nanoparticles (Sky Blue). It is evident from Fig. 4a that there is a strong linear correlation ($R^2 > 0.98$) between total fluorescence signal and applied fluorophore mass with a slope of 3.03×10^7 counts/s/μg. The intercept representing tissue autofluorescence was corrected for as described below. The repeatability of this method is ±9% as estimated from the scatter of the data around the linear curve fit in Fig. 4a. As this value is significantly larger than the estimated accuracy of the pulmonary fluorophore dose (gravimetric analysis as described above) we argue that 9% represents the accuracy of the Cryoslicing Imaging method.

As an example for a drug–fluorophore conjugate, we tested the method with FcγR-Alexa750. As experimental drugs are typically expensive, minimizing drug consumption is essential. Hence, we performed a single-point calibration with a bare minimum of two lungs. One untreated lung and one lung with 1.9 ± 0.3 μg of the drug–fluorophore conjugate (FcγR-Alexa750), where the uncertainty represents the repeatability of intratracheal dose application

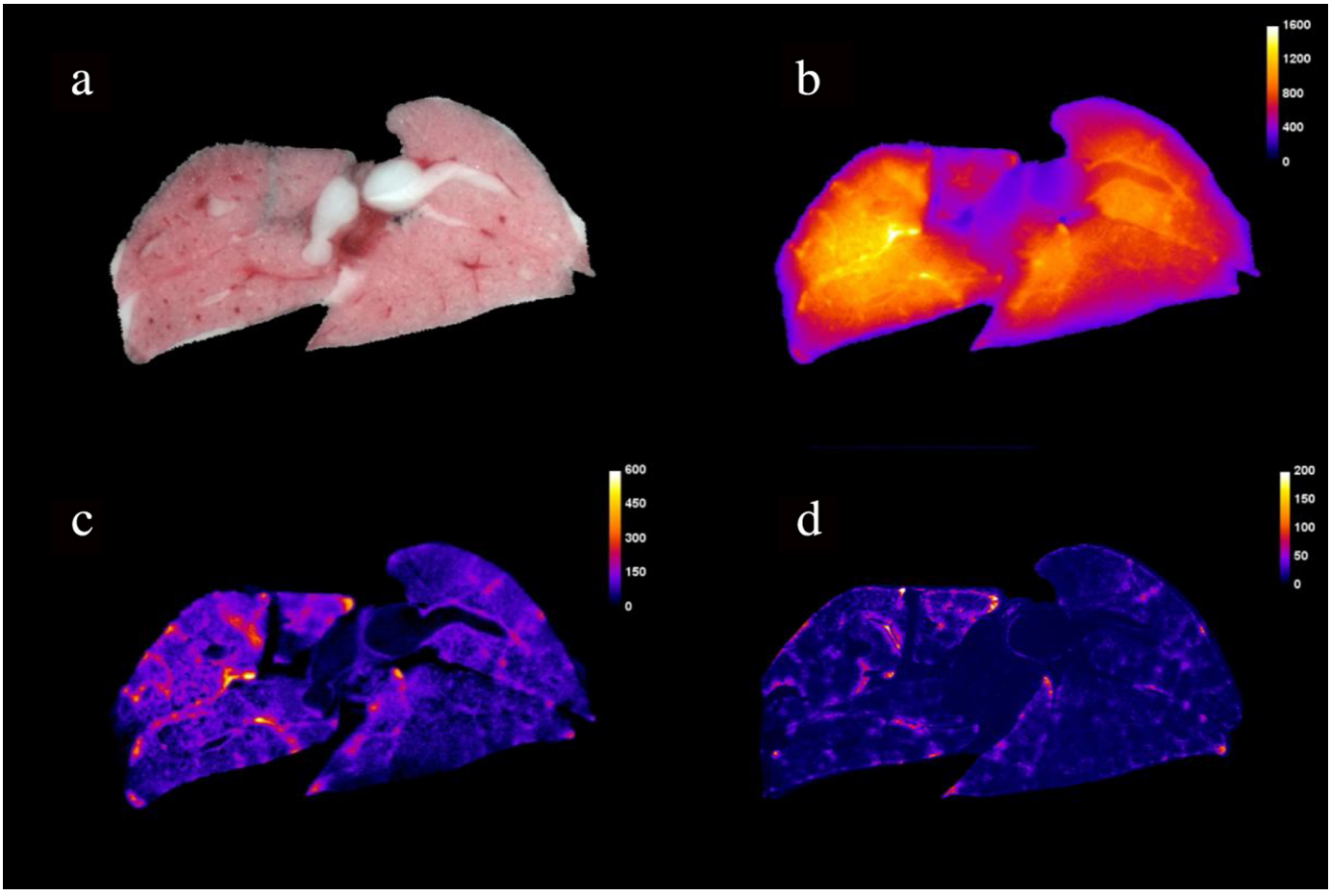

Fig. 3. Out-of-plane fluorescence correction. (a) A white light reflection image (RGB-color) of the block face of a frozen murine lung with the instilled fluorescence-labeled drug (FcγR-Alexa750). (b) The corresponding fluorescence intensity from the block face is shown in false colors. (c) The reconstruction of fluorescence contained in the top 100 μm slice from the two adjacent block face images accounting for sub-surface (out-of-plane) fluorescence. (d) Corresponding fluorescence intensity measured directly in a thin (25 μm) slice removed from the block face depicted in panel (a).

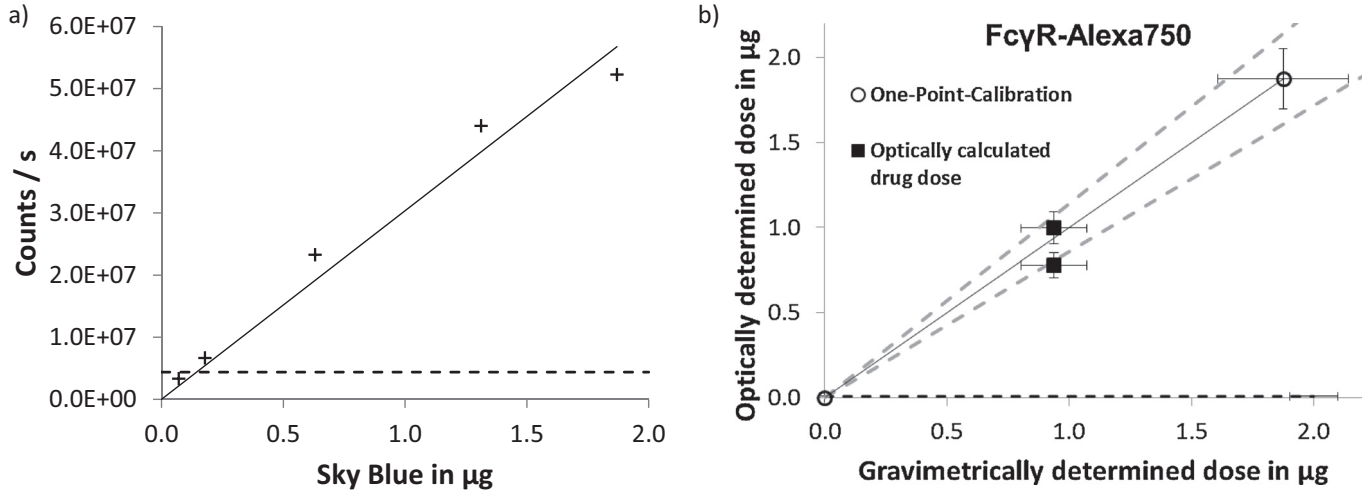

Fig. 4. (a) Dose–response curve for fluorescent nanoparticles (Sky Blue) demonstrating the linearity and detection limit of the method. Total pulmonary fluorescence counts for different doses of Sky Blue nanoparticles instilled into the lungs of mice are shown. The tissue autofluorescence signal was subtracted. The graph is showing a linear correlation between the total fluorescence signal from the murine lungs and applied dose of Sky Blue ($R^2 = 0.98$), where the slope of 3.03×10^7 counts/s/μg represents the intensity–mass conversion factor needed for quantitative Fluorescence Imaging of Sky Blue. The horizontal dashed–dotted line represents the experimentally determined limit of detection (0.44×10^7 counts/s corresponding to 145 ng Sky Blue). (b) Comparison of optically calculated and gravimetrically determined pulmonary dose of a fluorescence-labeled drug (FcγR-Alexa750) using the intensity–mass conversion factor (5.27×10^8 counts/s/μg). The intensity–mass conversion factor was obtained from the slope of one-point-calibration (circle symbols). It was used to convert the fluorescence signal into drug dose for the two lungs containing about 0.9 μg dye (square symbols). The optically calculated and gravimetrically determined doses are in good agreement. The horizontal dashed line represents the experimentally determined limit of detection (8.3 ng). The *x*-error bars represent the repeatability of the drug application procedure (14%). The *y*-error bars represent the accuracy of the Cryoslicing Imaging method (9%). The dashed lines along the linear fit represent the uncertainty in determination of the intensity–mass conversion factor.

into the lungs. Assuming linearity and correction for tissue autofluorescence (as described below) the calibration line can be forced through the origin yielding an intensity–mass conversion factor of $(5.27 \pm 0.75) \times 10^8$ counts/s/μg (Fig. 4b). The validity of the 1-point calibration method was tested by determining the fluorescence-based fluorophore dose for two additional lungs instilled with 0.94 ± 0.14 μg of the FcγR-Alexa750, where the standard deviation indicates the repeatability of intratracheal instillation (14%) without utilizing gravimetric analysis of the instillation wear prior and after instillation. Using the intensity–mass conversion factor determined above the inferred doses were 0.78 ± 0.07 μg and 1.00 ± 0.09 μg, where the uncertainty represents the measurement accuracy of Cryoslicing Imaging (9%). It is evident from Fig. 4b that the calculated doses of 0.78 ± 0.07 μg and 1.00 ± 0.09 μg, which differ by −17% and 6% from the gravimetrically determined dose (ordinate; 0.94 ± 0.14 μg), respectively, are within the expected combined measurement uncertainties of the Cryoslicing Imaging method (9%) and the instillation procedure (14%; here without gravimetric analysis of the pulmonary drug dose). This confirms the validity of the 1-point calibration method for FcγR-Alexa750. Hence, this method can be used to convert the measured fluorescence intensity into fluorophore mass for lungs which have received an unknown amount of drug during preclinical testing, for instance, *via* an inhalation procedure.

Finally, the limit of detection of this method was determined from the autofluorescence of four untreated lungs (lungs without fluorophore). The total pulmonary fluorescence signal from the untreated lungs was $(1.56 \pm 0.15) \times 10^7$ counts/s (mean ± SD, $n = 4$). The low relative standard deviation of 10% demonstrates the high degree of stability of the imaging and sample preparation procedure. The mean signal from the untreated lungs represents the mean tissue autofluorescence and was therefore subtracted from the data presented in Fig. 4a and b. Typically the limit of detection is defined as the 3σ noise level (3-fold standard deviation) about the zero point. With the slopes (intensity–mass conversion factors) determined in Fig. 4a and b the 3σ noise level of 0.44×10^7 counts/s corresponds to a detection limit of 145 ng and 8.3 ng for Sky Blue and FcγR-Alexa750, respectively. This analysis shows that all FcγR-Alexa750 samples were above the limit of detection. On the other hand, the lowest applied Sky Blue dose of 71 ng is clearly below the detection limit and should therefore be considered equal to zero within the statistical limits of the Cryoslicing Imaging method presented here.

4. Discussion

Lung deposition of inhaled substances is a two-sided coin. Pharmaceutical agents are used in inhalation therapy, but inadvertent inhalation of toxins or over-dosed drugs may also result in health risks. Both the therapeutic and toxic potential of substances depends not only on dose, but also on the region of deposition within the lungs [3]. Hence, there is a significant interest in monitoring the regional deposition of both nanocarriers and (molecular) drugs. Optical bioimaging has great potential for measuring spatially resolved tissue-delivered drug dose and probing complex biologic interactions in small animals such as mice. *In vivo* bioimaging will even allow for longitudinal real-time monitoring of disease progression and efficacy of treatment in the same animal, thus offering the potential to accelerate basic research and drug discovery and to reduce cost and the required number of animals [21]. In this proof-of-concept study we present and validate *ex vivo* Cryoslicing Imaging for quantitative 3D assessment of fluorophore dose in the lungs of mice.

The linearity of quantitative Cryoslicing Imaging can be seen from Fig. 4a using fluorescent nanoparticles Sky Blue. This is the prerequisite for reliable and simple application of this method even for cost-intensive investigational drugs. An excellent linear relationship between the measured total fluorescence signal and the corresponding amount of pulmonary fluorophore suggests that the simple image processing algorithm presented here provides quantitatively valid data. As the dose–response curve is linear and has an intercept close to zero (after the autofluorescence signal was subtracted), the intensity–mass conversion factor for the precious fluorophore–drug conjugate can be obtained by preparing at least one "reference" lung containing a realistically distributed and known amount of fluorophore and one without any fluorophore (autofluorescence of tissue). Of course using a larger number of reference lungs will improve the dosimetric accuracy of the method. As shown here the required reference lung(s) can be prepared using the intratracheal instillation method combined with gravimetric analysis of the instillation wear described above.

For validation of the method we have chosen Sky Blue as surrogate drug, because its spectral range is in the NIR optical window of tissue imaging and its fluorophore is embedded in a polystyrene latex matrix, which guarantees stable quantum yield independent of the microenvironment of the Sky Blue nanoparticles. The situation is potentially more complicated for a fluorescence-labeled molecular drug, as the covalently bound fluorophore may interact with proteins and enzymes of the biological matrix which may change the quantum yield of the fluorescence tracer in an unpredictable way. However, no such complications were observed for FcγR labeled with Alexa750, an experimental drug currently under preclinical investigation. Applying the 1-point calibration technique described above, the pulmonary mass doses for two reference lungs containing known amounts of FcγR-Alexa750 was obtained by the Cryoslicing Imaging method (Fig. 4b). Taking into account the accuracy of the Cryoslicing Imaging method and the repeatability of the pulmonary application of reference doses, there is a good agreement between the fluorescence-based and the known pulmonary dose. Hence, the Cryoslicing Imaging technique can be used for quantitative assessment of drug dose in murine lungs. Obviously, the accuracy of the calibration curve can be improved by using a larger number of reference lungs. Furthermore, the accuracy of the pulmonary dose in the reference lung can be enhanced from 14% to 5%, if the instillation wear is gravimetrically analyzed prior and after instillation as described above.

In general the photon yield of a fluorophore, and hence the corresponding intensity–mass conversion factor, depends on various parameters including type of fluorophore, optical properties of the frozen lung tissue as well as design and operational aspects of the Cryoslicing Imaging device. As fluorophores are typically used as labeling agent, the fractional contribution of the fluorophore to the substance mass strongly determines the intensity–mass conversion factor. Also other effects such as photo-bleaching or (self-) quenching of the fluorophore will affect the intensity–mass conversion factor. To account for all of these aspects the Cryoslicing Imaging technique has to be calibrated for each fluorophore. Since the experimental conditions, including the tissue optical properties (μ_{eff}) are kept constant for all the lungs, the quantification of fluorophore dose is fairly insensitive to any inaccuracy in the determination of the μ_{eff}.

Another important aspect is the limit of detection, which was determined from the variability of the fluorescence signal from four untreated lungs. The baseline value mainly depends on tissue autofluorescence, the ambient light in the room and the quality of the spectral filters and cross-talk of the filters due to partial reflection of the excitation light. The 3σ variability of the untreated lung signals defined the limit of detection as 8.3 ng and 144 ng for FcγR-Alexa750 and Sky Blue, respectively. With a maximum applied dose of 1.9 μg, our data document a dynamic measurement range of

more than two (229) and one order of magnitude (13) for FcγR-Alexa750 and Sky Blue, respectively, *i.e.*, pulmonary fluorophore doses as low as 0.44% and 7.6% of the maximum applied fluorophore mass can be detected for FcγR-Alexa750 and Sky Blue, respectively.

In this proof-of-concept study no efforts were made to improve the limit of detection. If measurements below the current detection limit are to be performed, the signal-to-noise ratio could be improved by *e.g.* using low fluorescence animal diet (reduces tissue autofluorescence), complete removal of the blood from the lungs (hemoglobin is expected to be the main source of autofluorescence in the lung) and/or by using different imaging settings, like multi wavelength imaging for spectral unmixing of the signal for improved removal of auto-fluorescence [17,22]. In addition, narrow band laser excitation and/or filters with less cross-talk and a better optical shielding of the imaging chamber may improve sensitivity.

In the method presented here a relatively simple, yet accurate, algorithm for the correction of out-of-plane fluorescence was applied, which does not involve direct modeling of light propagation in the tissue. However, even this correction algorithm is not necessary, if only individual slices (instead of block faces) would be imaged. This is typically not done due to technical difficulties such as the softness or brittleness of unfrozen or frozen organ slices, respectively, which makes it complicated to maintain the structural integrity of a single lung slice. For a few representative cases, individual 25 μm thick lung slices were imaged, but upon touching the object holder the slice immediately melts and loses its stiffness. As seen from Fig. 3c and d there is good agreement between the calculated and measured fluorescence distribution.

As perquisite for correct out-of-plane fluorescence correction the effective attenuation coefficient (μ_{eff}) of frozen murine lung tissue was experimentally determined as $10.0 \pm 0.6\ cm^{-1}$ (at 716 nm), which is relatively close to published values between 11 and $17\ cm^{-1}$ (at 633 or 790 nm) for non-frozen lung tissue from various animals other than mice [23]. To the best of our knowledge, this is the first experimental μ_{eff} value for a mouse lung and in particular for frozen murine lung tissue. A value of $\mu_{eff} = 10.0\ cm^{-1}$ implies that for 100 μm slices 90.5% of subsurface fluorescence is reaching the surface (out of a depth of 100 μm). This value decreases to 36.9% and 13.5% and 5.0% for a depth of 1 mm, 2 mm and 3 mm, respectively. As mouse lungs have a typical dimension of 1.5–2 cm, most of the light measured off the block face emanates from the top few millimeters of the sample. Obviously, these values depend on μ_{eff} and hence on the chosen wavelength. Our measurements were performed at 716 nm, which lies in the NIR wavelength regime (*ca.* 600–1000 nm), the so-called *optical window* where light–tissue interaction and hence μ_{eff} are minimal. While the method presented here is not limited to this wavelength range, its performance characteristics depend on the spectral range. For shorter wavelengths, the contribution from out-of-plane fluorescence decreases, but the tissue autofluorescence increases [23–26] having a negative effect on the detection limit. Fluorophores with longer wavelengths are typically not advisable due to their reduced photon yield and deterioration of optical properties of many optical components, which ultimately results in inferior signal-to-noise ratio and consequently reduced detection limit. Hence, the NIR wavelength regime (*ca.* 600–1000 nm) are best suited for quantitative fluorescence measurements in biological tissue. All of these aspects can be experimentally determined for any given fluorophore according to the procedure described in the present study.

Historically, 3D drug distributions have been measured with radio-imaging methods [27,28]. The main advantage of this approach is the relatively low attenuation of radioactive irradiation in biological tissue [29]. However, handling of radioactive materials requires special safety measures and – may be more importantly – radioactive methods are not suitable for determination of the bioactivity of a drug, since they are not sensitive to specific biological responses such as inflammation, cytokine release *etc.* Matrix-assisted laser desorption ionization imaging mass spectrometry (MALDI-IMS) has been recently employed for visualization and quantitative analysis of an antitumor drug in murine xenografts (10 μm thin) with high spatial resolution and sensitivity [30]. However, MALDI-IMS is not suitable for analyzing a whole organ such as murine lung, as only a small sample volume can be measured in a single run. *In vivo* imaging of internal organs with visible light typically requires multi-modal approaches, where optical imaging is combined with *e.g.* acoustic and/or gamma ray (CT) tomography. The additional information from the second imaging mode provides anatomic information which can be used to improve the 3D reconstruction algorithm by performing modeling of the propagation of light using organ-specific optical properties [31]. While these methods have been used for quantitative assessment of *e.g.* lung cancer lesions using integrin-targeting fluorescent probes, accurate 3D fluorophore dose measurements in the entire lung of mice (or other mammals) have not been performed, yet, due to the limited penetration depth of light and the particularly complicated optical properties of the lung. To the best of our knowledge, no optical imaging method for quantitative 3D assessment of the fluorophore dose in an entire mammalian lung has been presented, yet. Hence, the method presented here is expected to provide a valuable tool for accurate determination of both lung deposited fluorescence-labeled drug dose with a dose resolution at ng level and – if biosensitive fluorescent probes are used – the corresponding bioactivity of the drug.

5. Conclusions

This proof-of-concept study has shown that Cryoslicing Imaging can be used for quantitative 3D dose assessment of fluorescence-labeled drugs in the lungs of mice. The estimated measurement accuracy is 9% and the limit of detection was 144 and 8.3 ng for the fluorescent nanoparticles (Sky Blue) and fluorophore–drug conjugate (FCγR-Alexa750) used here, respectively. This is sufficiently low for many applications including assessment of dose and, possibly, bioactivity of inhaled drugs and nanocarriers into the lungs of mice. This method has the potential to serve as an accurate reference method for the development and validation of technologically more challenging quantitative *in vivo* imaging methods.

Acknowledgment

We would like the thank Dominik ter Meer for providing the soluble human Fcγ-receptor IIB (fluorescence-labeled).

Appendix A. Supplementary data

Supplementary data associated with this article can be found, in the online version, at http://dx.doi.org/10.1016/j.jpba.2014.09.001.

References

[1] J.S. Patton, P.R. Byron, Inhaling medicines: delivering drugs to the body through the lungs, Nat. Rev. Drug Discov. 6 (2007) 67–74.
[2] C.Y. Dombu, D. Betbeder, Airway delivery of peptides and proteins using nanoparticles, Biomaterials 34 (2013) 516–525.
[3] N.R. Labiris, M.B. Dolovich, Pulmonary drug delivery. Part I: physiological factors affecting therapeutic effectiveness of aerosolized medications, Br. J. Clin. Pharmacol. 56 (2003) 588–599.
[4] M.B. Dolovich, R. Dhand, Aerosol drug delivery: developments in device design and clinical use, Lancet 377 (2011) 1032–1045.
[5] M. Königshoff, O. Eickelberg, WNT signaling in lung disease a failure or a regeneration signal? Am. J. Resp. Cell Mol. 42 (2010) 21–31.
[6] M. Königshoff, S. Saglani, B.J. Marsland, O. Eickelberg, Rebuilding a diseased lung: repair and regeneration, Eur. Respir. J. 41 (2013) 497–499.

[7] R.J. MacLoughlin, B.D. Higgins, J.G. Laffey, T. O'Brien, Optimized aerosol delivery to a mechanically ventilated rodent, J. Aerosol Med. Pulm. Drug D 22 (2009) 323–332.
[8] Y. Cai, L. Zhu, F. Zhang, G. Niu, S. Lee, S. Kimura, X. Chen, Noninvasive monitoring of pulmonary fibrosis by targeting matrix metalloproteinases (MMPs), Mol. Pharmacol. 10 (2013) 2237–2247.
[9] V. Ntziachristos, J. Ripoll, L.V. Wang, R. Weissleder, Looking and listening to light: the evolution of whole-body photonic imaging, Nat. Biotechnol. 23 (2005) 313–320.
[10] A. Ale, V. Ermolayev, E. Herzog, C. Cohrs, M.H. de Angelis, V. Ntziachristos, FMT-XCT: in vivo animal studies with hybrid fluorescence molecular tomography-X-ray computed tomography, Nat. Methods 9 (2012) 615–620.
[11] R. Richards-Kortum, E. Sevick-Muraca, Quantitative optical spectroscopy for tissue diagnosis, Annu. Rev. Phys. Chem. 47 (1996) 555–606.
[12] A. Bogaards, H.J.C.M. Sterenborg, B.C. Wilson, In vivo quantification of fluorescent molecular markers in real-time: a review to evaluate the performance of five existing methods, Photodiagn. Photodyn. 4 (2007) 170–178.
[13] A. Mazhar, D.J. Cuccia, S. Gioux, A.J. Durkin, J.V. Frangioni, B.J. Tromberg, Structured illumination enhances resolution and contrast in thick tissue fluorescence imaging, J. Biomed. Opt. 15 (2010), 010506-1–010506-3.
[14] D. Wilson, D. Roy, G. Steyer, M. Gargesha, M. Stone, E. McKinley, Whole mouse cryo-imaging, Proc. SPIE 6916 (2008), 69161I–69161I-9.
[15] M. Omar, S. Kellnberger, G. Sergiadis, D. Razansky, V. Ntziachristos, Near-field thermoacoustic imaging with transmission line pulsers, Med. Phys. 39 (2012) 4460–4466.
[16] J.A.E. Spaan, R. ter Wee, J.W.G.E. van Teeffelen, G. Streekstra, M. Siebes, C. Kolyva, H. Vink, D.S. Fokkema, E. VanBavel, Visualisation of intramural coronary vasculature by an imaging cryomicrotome suggests compartmentalisation of myocardial perfusion areas, Med. Biol. Eng. Comput. 43 (2005) 431–435.
[17] A. Sarantopoulos, G. Themelis, V. Ntziachristos, Imaging the bio-distribution of fluorescent probes using multispectral epi-illumination Cryoslicing Imaging, Mol. Imaging Biol. 13 (2011) 874–885.
[18] G.J. Steyer, D. Roy, O. Salvado, M.E. Stone, D.L. Wilson, Removal of out-of-plane fluorescence for single cell visualization and quantification in cryo-imaging, Ann. Biomed. Eng. 37 (2009) 1613–1628.
[19] R.H. Brown, D.M. Walters, R.S. Greenberg, W. Mitzner, A method of endotracheal intubation and pulmonary functional assessment for repeated studies in mice, J. Appl. Physiol. 87 (1999) 2362–2365.
[20] A.A. Götz, J. Rozman, H.G. Rodel, H. Fuchs, V. Gailus-Durner, M.H. de Angelis, M. Klingenspor, T. Stoeger, Comparison of particle-exposure triggered pulmonary and systemic inflammation in mice fed with three different diets, Part. Fibre Toxicol. 8 (2011) 30.
[21] M. Murata, K. Tahara, H. Takeuchi, Real-time in vivo imaging of surface-modified liposomes to evaluate their behavior after pulmonary administration, Eur. J. Pharm. Biopharm. 86 (2014) 115–119.
[22] L. Zhou, W.S. El-Deiry, Multispectral fluorescence imaging, J. Nucl. Med. 50 (2009) 1563–1566.
[23] J.F. Beek, P. Blokland, P. Posthumus, M. Aalders, J.W. Pickering, H.J.C.M. Sterenborg, M.J.C. van Gemert, In vitro double-integrating-sphere optical properties of tissues between 630 and 1064 nm, Phys. Med. Biol. 42 (1997) 2255–2261.
[24] G.C. Tang, A. Pradhan, R.R. Alfano, Spectroscopic differences between human cancer and normal lung and breast tissues, Lasers Surg. Med. 9 (1989) 290–295.
[25] J. Hung, S. Lam, J.C. Leriche, B. Palcic, Autofluorescence of normal and malignant bronchial tissue, Lasers Surg. Med. 11 (1991) 99–105.
[26] A. Roggan, M. Friebel, K. Dörschel, A. Hahn, G. Müller, Optical properties of circulating human blood in the wavelength range 400–2500 nm, J. Biomed. Opt. 4 (1999) 36–46.
[27] J.S. Fleming, J.H. Conway, Three-dimensional imaging of aerosol deposition, J. Aerosol Med. 14 (2001) 147–153.
[28] M.B. Dolovich, 18F-fluorodeoxyglucose positron emission tomographic imaging of pulmonary functions, pathology, and drug delivery, Proc. Am. Thorac Soc. 6 (2009) 477–485.
[29] J.S. Fleming, A technique for using CT images in attenuation correction and quantification in SPECT, Nucl. Med. Commun. 10 (1989) 83–97.
[30] M. Yasunaga, M. Furuta, K. Ogata, Y. Koga, Y. Yamamoto, M. Takigahira, Y. Matsumura, The significance of microscopic mass spectrometry with high resolution in the visualisation of drug distribution, Sci. Rep. 3 (2013) 3050.
[31] V. Ntziachristos, Going deeper than microscopy: the optical imaging frontier in biology, Nat. Methods 7 (2010) 603–614.